Distortional elastic buckling for aluminium: Available prediction models versus design specifications

N. Kutanova

Eindhoven University of Technology, the Netherlands

T. Peköz

Cornell University, USA

F. Soetens

Eindhoven University of Technology, the Netherlands

TNO Built Environment and Geosciences, the Netherlands

Accurate prediction of buckling behaviour of aluminium structural elements with thin-walled cross-sectional shapes is important for efficient design. Many recent investigations in terms of cross-sectional instability have proved that distortional buckling has a substantial effect on the structural behaviour of aluminium thin-walled members. Aluminium design rules are limited regarding the distortional buckling phenomenon and simplified to meet the theoretical solutions of the plate-buckling problem. However, the plate buckling problem does not reflect the real cross-sectional instability behaviour because the edge restrained conditions of each plate element are not taken into account. In this respect, prediction models like the Direct Strength Method which is based on the elastic buckling solutions for the entire cross-section can achieve these requirements. In order to provide a reliable design approach specifically for aluminium, a new prediction model for distortional buckling of C-shaped thin-walled cross-sections has been developed (Kutanova model [2009]). This model is based on advanced non-linear finite element analyses that include the interaction of cross-sectional plate elements. In this study, the distortional bucking resistance of C-sections has been calculated according to the current design rules (AA Specification and Eurocode 9) and two prediction models: the Direct Strength Method and the Kutanova model. The calculations using these different approaches mainly show the inconsistencies in results provided by the aluminium design standards compare to the prediction models.

 Keywords: Distortional buckling, aluminium, thin-walled cross-sections, design specification, buckling

1   Introduction

Aluminium extrusions are of interest for different industrial fields such as structural applications and transport. The extrusion process allows one to optimize structural elements according to the design requirements with a relative ease. Optimization of the shape of the aluminium elements often results in the use of thin-walled cross-sectional shapes, which increases the complexity of the cross-section. For thin-walled elements, cross-sectional instability - in particular local and distortional buckling - has a substantial effect on the structural behaviour.

In classification of cross-sectional instability local buckling implies changes in geometry with the points of intersection between the plate elements of the section remaining straight, while distortional buckling involves changes in the cross-sectional geometry with points of intersection not remaining straight. The current design rules (Eurocode 9 [2007], AA Specification [2005]) used by engineers are limited to local buckling of simple and symmetrical cross-sections. Design standards consider the cross-sectional instability as the buckling of individual plate elements which compose the cross-section and do not consider the interaction of the cross-sectional plates. Distortional buckling is covered indirectly by formulas for edge stiffened elements. These design rules do not provide an accurate description of distortional buckling behaviour and can not be used for more complex shapes.

An extensive study into distortional buckling of aluminium extrusions has been carried out by Kutanova [2009] resulting in a prediction model for the calculation of the ultimate resistance of uniformly compressed C-sections subjected to cross-sectional instability. Finite Element (FE) modelling has been used for a detailed investigation of the actual distortional buckling behaviour and local-distortional interaction. It has been validated by experiments that the FE-model is a useful tool for the prediction of structural behaviour of uniformly compressed aluminium members with various cross-sectional shapes.

The goal of this paper is to present a comparison analysis between the current aluminium design standards and the prediction models. In the current work, the commonly used Direct Strength Method (Schafer [2006a]) for the distortional buckling prediction of the steel elements is adapted to aluminium. Results of calculations of distortional elastic bucking resistance of various C-sections according to the finite element analysis, current design rules (Eurocode 9, AA Specification) as well as the adapted Direct Strength Method and the Kutanova model are presented.

2   C-shaped aluminium columns

2.1   Selection of the cross-sectional shape for distortional buckling

The appropriate specimen selection for distortional buckling investigation is achieved using the CUFSM program based on the Finite Strip Method (Schafer [2006b]). The selected cross-sectional shape should be able to provide the development of distortional buckling avoiding the occurrence of local and overall buckling.

Distortional buckling is known as a flange-stiffener phenomenon (Hancock [1978]). Therefore, it is proposed to select a simple symmetrical shape with flange stiffeners. The commonly used C-shaped profile is selected. To allow dominance of distortional buckling and not local buckling, the length of the flange stiffener is taken small. To exclude any occurrence of local buckling, the thickness of the web is twice as thick as the thickness of flanges and lips. An example of the CUFSM signature curve and the deformed shape for the C-shaped profile as a result of the finite strip analysis is given in Figure 1.
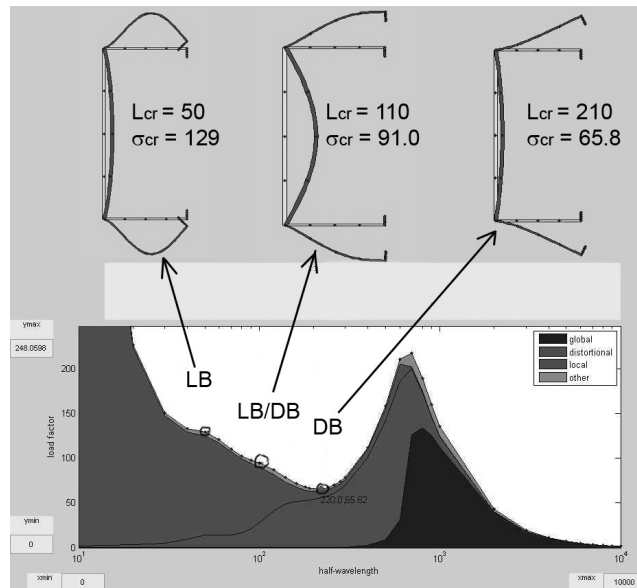

Figure 1: CUFSM results for selected C-profile with defined buckling
shapes for local and distortional modes

It can be noticed from the CUFSM results that local buckling might occur and not only distortional buckling. Figure 1 shows the occurrence of the local buckling mode and shows the resulting local buckling shapes. Critical points for local buckling are not defined

by the CUFSM, but visible on the signature curve. Hence, critical points for local buckling are indicated manually. Figure 2 specifies one distortional signature curve, one curve for local/distortional interaction when local buckling governs and one signature curve for local buckling. It means that distortional buckling initiates first and local buckling governs later. This observation is very important for the prediction of cross-sectional instability behaviour.
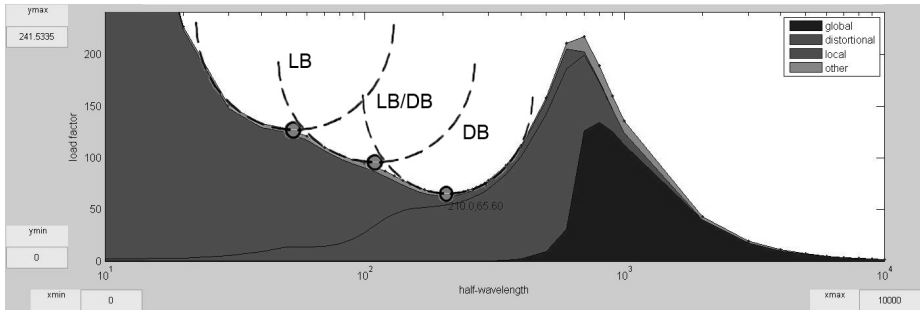

Figure 2: CUFSM results for selected C-profile with defined buckling curves and critical points for local and distortional modes

Based on the CUFSM results of Figure 1 and Figure 2 it can be concluded that in this example distortional buckling is initiated first, while local/distortional interaction and local buckling proceeds later. Thus, this C-shaped specimen is an appropriate choice for the distortional buckling study.

2.2 *Characteristics of the considered C-shaped specimens*

Figure 3 shows the selected profile. Table 1 gives the dimensions for the considered C-shaped specimens in accordance with Figure 3.

Specimen designation is in line with the specification. The first number corresponds to the value of thickness for flanges and lips, while the second number in brackets relates to the value of thickness for the web. The letter indicates the shape of the profile: "C" for C-shaped profile. The last number is the cross-sectional stiffener length (or value *c* in the table).

It should be noted that the total length of the specimens (*L*) is selected three times the critical distortional buckling wavelengths according to Kutanova [2009].
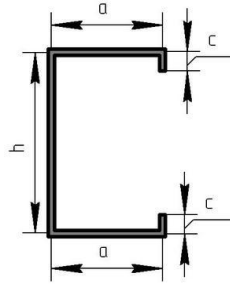
Figure 3: Selected cross-sectional shape

Table 1: C-shaped specimens specifications

No.	Specimen	$h[mm]$	$a[mm]$	$c[mm]$	$t_h[mm]$	$t_a[mm]$	$t_c[mm]$	$L[mm]$
1	2.5(3)C5	100	50	5	3	2.5	2.5	510
2	1(2)C10	100	50	10	2	1	1	1050
3	2(2.5)C5	100	50	5	2.5	2	2	540
4	1(2)C7.5	100	50	7.5	2	1	1	870
5	1.5(2)C5	100	50	5	2	1.5	1.5	600
6	1(2)C5	100	50	5	2	1	1	630
7	0.75(2)C5	100	50	5	2	0.75	0.75	720
8	0.75(1.5)C5	100	50	5	1.5	0.75	0.75	750

Table 2: CUFSM results for C-shaped specimens (6082-T6 aluminium alloy proof stress is considered $f_{0.2} = 250$ [N/mm²])

No.	Specimen	$L_{cr;l1}$ [mm]	$\sigma_{cr;l1}$ [N/mm²]	$L_{cr;l2}$ [mm]	$\sigma_{cr;l2}$ [N/mm²]	$L_{cr;d}$ [mm]	$\sigma_{cr;d}$ [N/mm²]
1	2.5(3)C5	70	270	-	-	170	160
2	1(2)C10	90	106	40	140	350	136
3	2(2.5)C5	90	166	-	-	180	119
4	1(2)C7.5	100	105	40	139	290	102
5	1.5(2)C5	100	109	-	-	200	84
6	1(2)C5	100	97	40	133	210	70
7	0.75(2)C5	40	78	-	-	240	57
8	0.75(1.5)C5	100	58	-	-	250	49

Table 2 contains the CUFSM resulting critical lengths and critical stresses for all the specimens. Similar to Figure 1, critical points are visually defined for the local buckling mode. For some specimens two critical points for local buckling can be distinguished. Thus, critical values for the local buckling mode ($L_{cr;l1}$, $\sigma_{cr;l1}$); ($L_{cr;l2}$, $\sigma_{cr;l2}$) and critical values for the distortional buckling mode ($L_{cr;d}$, $\sigma_{cr;d}$) are included in the table. It can be noticed in Table 2 that in all cases distortional buckling initiates first, except for the second specimen 1(2)C10 where the initial buckling is local buckling.

3 Numerical FEM tool

3.1 Description of the Finite Element model

A finite element model is a useful tool for prediction of the structural behaviour of uniformly compressed aluminium members with various cross-sectional shapes. Simulation of compression tests for the specimens of Table 1 are executed using a finite element model, validated by experimental results (see Kutanova [2009]).

The test specimens are simulated using so-called CQ40S eight-node curved shell elements. The curved shell elements in DIANA (Hendriks [2007]) are based on iso-parametric solid approach by including the following shell theory hypothesis: normals remain straight, but not necessarily normal to the reference surface; the normal stress in the normal direction is equal to zero. Each node has three translations as well as two rotations (the rotation in normal direction is not included); a total of 40 degrees of freedom exist.

A quadratic interpolation and Gauss integration scheme is applied for each element. Seven integration points have been applied over the plate thickness, in each of the 2*2 in-plane shell integration points. Note that the calculation time increases linearly with the number of thickness integration points. However, the accuracy of the described stress-pattern improves significantly when a number of seven is taken instead of default number of three. Existing work by Mennink [1999] (with 3, 7 and 9 thickness integration points) shows that the number of seven is sufficiently accurate.

The model and mesh of the specimen are generated using the actual dimensions of the test specimens (see Table 1). For the considered C-shaped specimen, the following mesh refinement provides a sufficiently accurate result: 20 elements in the web, 10 elements in each flange and one or two elements in each stiffener depending on the size of the stiffener. The size of the element in longitudinal direction is maximum 33 mm.

The model is supported at both the "bottom" and the "top" edges of the specimen. All translations and rotations at the bottom and the top edges are restricted. Thus, the column

is modelled to resemble a two-sided fixed column. The axial load is applied as a uniform axial displacement (u).

Imperfections in the shape of the first Euler buckling mode are introduced into the FE-model. It has been observed that applying imperfections in the shape of the first Euler buckling mode is safe, comparing to application of the real imperfection pattern. To recognize the pure distortional buckling behaviour the influence of imperfections is minimized by applying a very small imperfection, 1/1000 of the plate thickness. The application of such imperfections is convenient, because the size of actual imperfections is small for aluminium extrusions. In Kutanova [2009], the influence of the value of imperfections is found less than 2% and can be neglected.

3.2   FE-results for the C-shaped specimen

The CUFSM output screen is shown before in Figure 1 for the specimen No.6 of Table 1. According to the CUFSM calculations, distortional buckling is initiated first, whereas for higher stresses two critical points for local buckling are present. It is assumed that secondary buckling of the cross-section is the local buckling of the web, which corresponds to the most critical point for local buckling. The manually defined second critical point for local buckling is considered as well to check if it has any physical meaning.
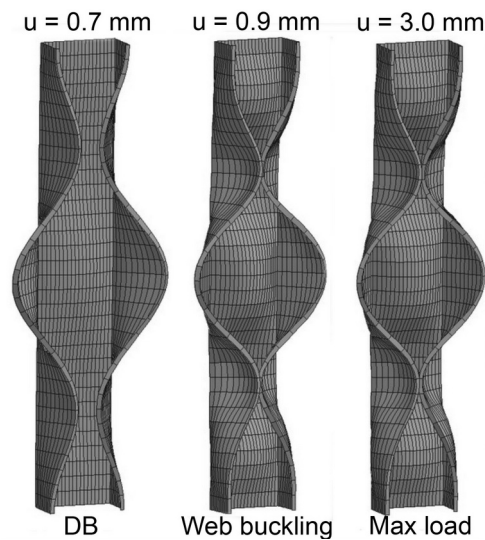

u = 0.7 mm   u = 0.9 mm   u = 3.0 mm

DB   Web buckling   Max load

Figure 4: FEM deformed shapes for C-shaped specimen: local and distortional buckling

The resulting deformed specimens according to the FEM non-linear analysis are shown in Figure 4. The specimen is subjected to pure distortional buckling first and later local buckling occurs, which can be noticed by the deformed shapes. The specimen failed due to distortional-local buckling.

Results of the FE-analysis are plotted in Figure 5. Based on the CUFSM results, three critical points have been defined. The critical values for initial distortional buckling, local buckling and manually defined secondary local buckling are included in the load-deflection graph. According to the load-deflection diagram, the second critical value for local buckling does not indicate any effect on the buckling behaviour.
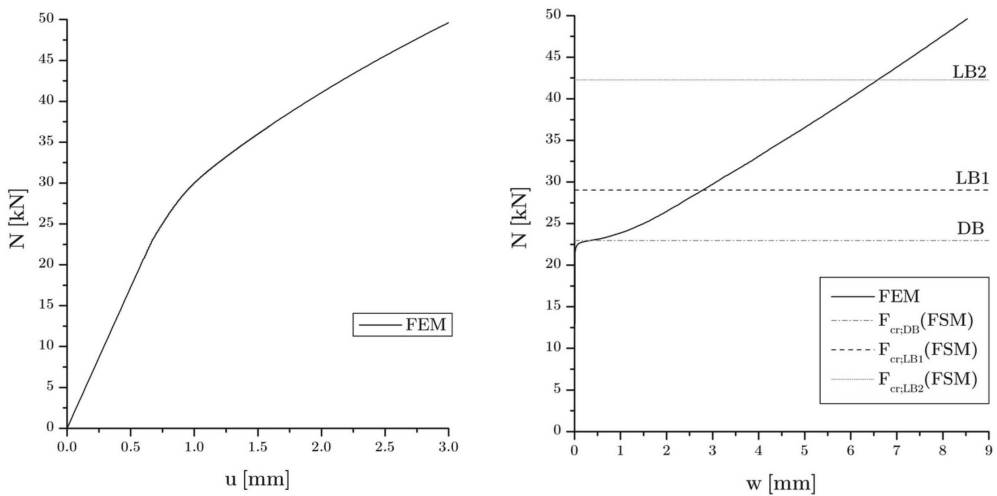

Figure 5: Load-displacement (left) and load-deflection (right) plots for considered C-specimen.

The FE-model results for the web, outstanding group (flange+lip) and the whole section 1(2)C5 are represented in Figure 6. Figure 6 shows that initial buckling occurs at the critical stress $\sigma_{cr;d}$ due to instability of the outstanding element. Secondary buckling or buckling of the web is well-defined from the CUFSM results (see Figure 2). Again, no particular influence of the second critical value for local buckling can be recognized. Therefore, it is concluded that only two CUFSM results should be considered: initial buckling and manually indicated secondary buckling (which is the most critical after initial buckling).

Figure 7 shows the relationship between the tangential stiffness E^* and the axial strain ε^* for the plate elements and the whole C-section. Initial buckling develops when the critical point ($\varepsilon^* = 1$) is reached, which results in a gradual decrease of stiffness for the web and

258

section and a sudden drop for flange/stiffener assemblies. A subsequent load increase results in secondary buckling of the web. Mode jumping from distortional mode into local mode is not observed. Specimen failure is attributed to distortional-local interaction.
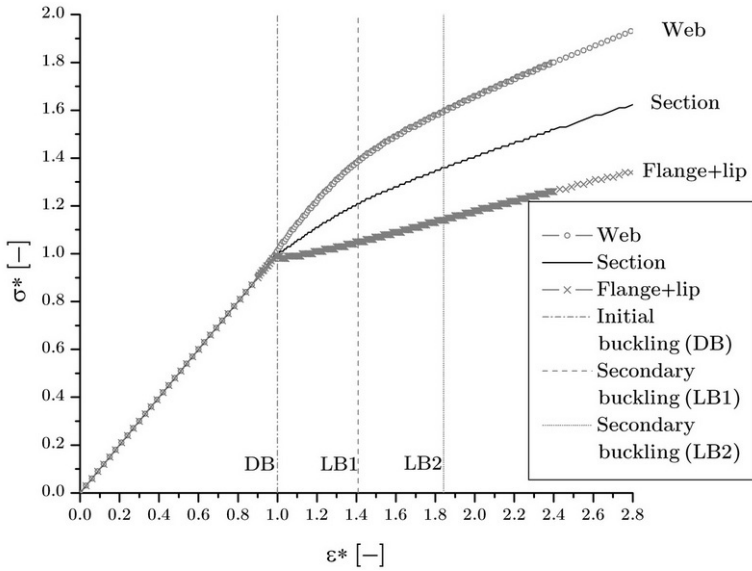

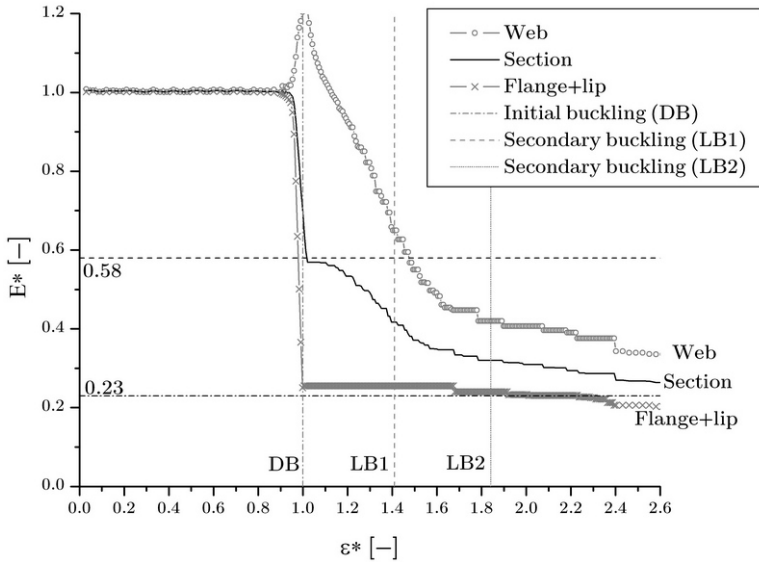*Figure 6: FE-results for plate elements of the considered C-specimen.*

Figure 7: Tangential stiffness for plate elements of the considered C-specimen.

Based on the represented results, it can be concluded that the finite element analyses results of the listed specimens can be used for the development of the prediction model for the elastic distortional buckling behaviour. Secondary buckling of the web is predicted by the Finite Strip Method (FSM). A perfect agreement has been found between FSM and FEM results for secondary buckling of the web. Thus, the CUFSM results can be used for the initial buckling prediction and also for the secondary buckling prediction.

4   Existing aluminium design rules

For all types of structures, analytical design rules are used to calculate the structural resistance. Cross-sectional instability and, in particular, distortional buckling influences the stability of the whole structure. There are several codes on aluminium structures which deal with the aspect of local and to a minor extent distortional buckling. The commonly used approach in Europe is given in Eurocode 9 [2007], described by Mazzolani [1985]. The cross-section is usually seen as a number of plates connected by nodes; interaction of cross-sectional plates is not taken into account.

Three different types of elements are recognized in a cross-section: flat outstand, flat internal and curved internal elements. The basic parameter is the slenderness parameter or the width-to-thickness ratio ($\beta = b/t$) of each element. Distortional buckling of C-shaped sections is considered as the buckling mode of the reinforced part of the cross-section (see section 6.1.4.3 in Eurocode 9). For distortional buckling of the reinforced parts value of η is introduced in the calculation of the slenderness parameter:

$$\beta = \eta \; \frac{b}{t} \, . \qquad\qquad (1)$$

A similar approach is used in the AA Specification [2005].

5   Recent analytical tools for distortional buckling prediction

5.1   Adapted Direct Strength Method

Based on the distortional design curve developed by Hancock et al. [1994], Schafer and Peköz [10] developed a Direct Strength Method (DSM). DSM was implemented and is fully described in design standards for cold-formed steel: AISI (Schafer [2006a]) and

AS/NZS [2005]. The DSM assumes a buckling load or moment for the whole section either as local or distortional buckling. If the mode is distortional, then the distortional buckling strength N_{cd} is computed by equations 2, 3 and 4:

For $\lambda_d > 0.561$
$$N_{cd} = N_y \qquad\qquad (2)$$

For $\lambda_d > 0.561$
$$N_{cd} = \left[1 - 0.25 \left(\frac{N_{od}}{N_y} \right)^{0.6} \right] \left(\frac{N_{od}}{N_y} \right)^{0.6} N_y{}' \qquad (3)$$

where the non-dimensional slenderness is given by:

$$\lambda_d = \sqrt{\frac{N_y}{N_{od}}} \,. \qquad\qquad (4)$$

The load $N_y = A f_y$ is the squash load of a section and the load N_{od} is the elastic distortional buckling load.

The original DSM equations were calibrated for steel. An attempt was made in the present study to apply an adapted DSM to the types of aluminium sections studied.

The distortional buckling loads according to FEM are plotted in Figure 8. In the current investigation, three aluminium alloys which are commonly used in structural applications are considered: 6082-T6, 6060-T66 and 5083-H111. This adapted version of DSM equation for distortional buckling is shown in Figure 8.
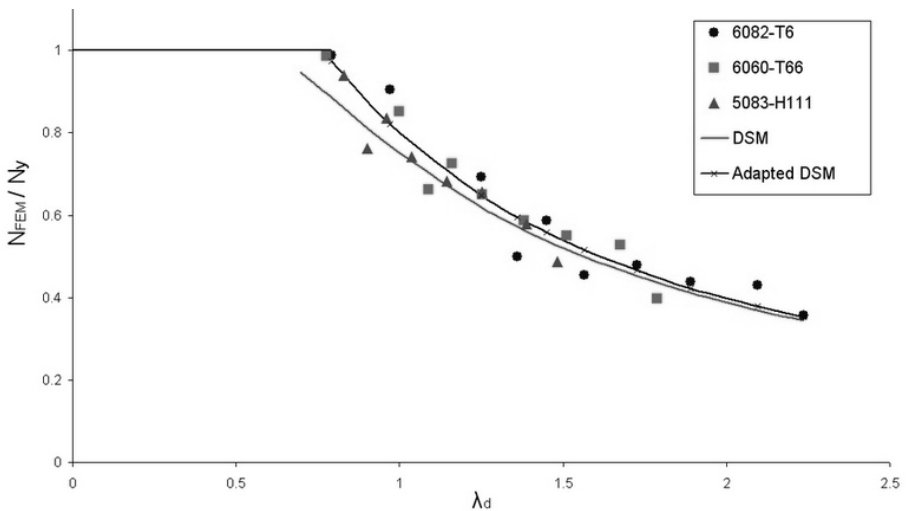

Figure 8: FEM results for distortional buckling and the proposed design curves

Thus, if the mode is distortional, then the adapted DSM Equations are:

For $\lambda_d > 0.561$ $\qquad\qquad\qquad N_{cd} = N_y$ $\qquad\qquad\qquad$ (5)

For $\lambda_d > 0.561$ $\qquad\qquad\qquad N_{cd} = \left[1 - 0.2\left(\dfrac{N_{od}}{N_y}\right)^{0.65}\right]\left(\dfrac{N_{od}}{N_y}\right)^{0.65} N_y{}'$ $\qquad$ (6)

where the non-dimensional slenderness is given by Equation 4.

As it was mentioned before, there is one specimen 1(2)C10 for which local buckling initiates first and distortional buckling is the secondary buckling. For local buckling strength prediction of this specimen, the design approach for local buckling according to AA Specification is used. However, in section 4.7.4 of AA Specification for interaction of local and overall buckling, the overall buckling should be substituted with distortional buckling as far as the local-distortional interaction takes place. Therefore, the CUFSM distortional buckling stress is used instead of the elastic critical stress.

5.2 *Kutanova / Mennink's model*

In Kutanova [2009], a prediction model for distortional buckling of C-shaped specimens is developed based on the actual buckling behaviour following the concept of Mennink's model for local buckling prediction (Mennink [2002]).

General ideas

The concept of Mennink's model is based on the interaction of cross-sectional plate elements. A cross-section is divided into: plate elements that buckle (group I) and plates that provide support (group II). Figure 6 illustrates these two groups of plates: group I is the web, group II is the outstanding flange/lip assembly. Plate elements with the critical buckling stresses lower than the critical buckling stress of the whole cross-section belong to plate group I. It is assumed that after the proportional limit is reached immediate failure occurs (inelastic buckling). Concerning plate group II, two situations are distinguished: plate group II behaves elastically until the proportional limit of the material or buckling of the plate group II occurs. Buckling of the plate group II is called secondary buckling. The post-buckling strength after secondary buckling is limited to the proportional limit. Therefore, initial and secondary buckling modes have to be defined for the cross-section.

262

An illustration of the local buckling behaviour of the cross-section is given in Figure 9. It can be seen that the section behaves elastically until the first critical point is reached (ε_{cr1}). Local buckling of the plate group I occurs, resulting in stiffness reduction. The post-buckling strength of plate group I is limited with the proportional limit of the material (ε_p): line "LL" in the figure. Plate group II behaves elastically until the second critical point is reached (ε_{cr2}), where local buckling of the plate group II happens. The post-buckling strength of the plate group II is limited with the material proportional limit, where failure occurs.
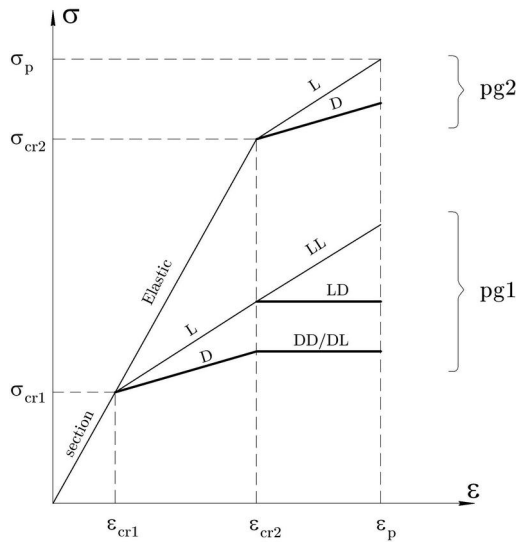

Figure 9: Illustration of the local and distortional buckling behaviour of the cross-section, according to Kutanova/Mennink model

The general ideas for distortional buckling behaviour are illustrated in Figure 9 together with local buckling behaviour. It is assumed that distortional buckling behaviour is similar to local buckling behaviour described above. However, the post-buckling strength for distortional buckling is lower than in case of local buckling, which can be noticed from the figure. The post-buckling strength for distortional buckling of plate group I is influenced by the secondary buckling initiation of plate group II: line "DD" in the figure. When the secondary buckling of plate group II is reached, no additional support is provided for plate group I. As a safe approach, it is assumed that there is no post-buckling strength for plate group I after the secondary distortional buckling. Therefore, the post-buckling

strength for plate group I is limited with the secondary distortional buckling stress of plate group II.

Local-distortional and distortional-local interactions are also represented in the figure, according to research of Kwon and Hancock [1992]. If initial buckling corresponds to local buckling and secondary buckling to distortional buckling, the post-buckling strength for local buckling of plate group I is limited with the secondary distortional buckling stress of plate group II (line "LD"). Vice versa for distortional-local interaction, the post-buckling strength for distortional buckling of plate group I is limited with the secondary local buckling stress of plate group II (line "DL").

Prediction model for distortional buckling behaviour of C-shaped aluminium structural elements
Discussion in this section is limited to distortional buckling prediction. Key aspect of the model is the application and determination of the actual critical stresses due to initial buckling (distortional buckling) and secondary buckling (local buckling). The input data for distortional buckling prediction are: $L_{cr;d}$ - the critical length for distortional buckling initiation, $\sigma_{cr;d}$ - the critical stress for distortional buckling initiation, the cross-sectional dimensions and the material properties. If local-distortional interaction takes place for a profile considered (specimen 1(2)C10), the input data will include the critical length and stress for local buckling development and Mennink's model [2002] for local buckling is applied, limiting the post-buckling strength for local buckling with the distortional buckling stress.

The above results in the following calculation procedure for distortional buckling:

[1] Determine the eigenvalue by either using analytical solutions or, more appropriate for arbitrary cross-sections, finite-element or finite-strip calculations. This results in the determination of the critical length $L_{cr;d}$ and the critical stress $\sigma_{cr;d}$ of the cross-section. The resulting buckling shape indicates that flange-stiffener or, in other words, distortional buckling occurs.

[2] Determine the secondary critical buckling stress by CUFSM. Local buckling proceeding after distortional buckling implies secondary buckling of the internal elements of the cross-section. The most critical local buckling stress defined on the CUFSM curve is related to the secondary buckling stress. Therefore, two plate groups are determined:

- The first plate group (pg1) consists of all outstanding plate elements (flange-stiffener assembly) that buckle at the initial critical stress for distortional buckling $\sigma_{cr;d}$.

- The second plate group (pg2) consists of all internal plates (web) that buckle at the secondary buckling critical stress for the local mode $\sigma_{cr;l}$.

[3] For each plate i of plate group I and plate j of plate group II, the cross-sectional area is determined from their plate width and thickness. Subsequently, this results in the following representations of the cross-sectional areas:

Plate group I $\qquad A_{pg1} = \sum_i b_i t_i$

Plate group II $\qquad A_{pg2} = \sum_j b_j t_j$

Cross-section $\qquad A = A_{pg1} + A_{pg2}$

[4] It is assumed that the proportional limit of the material, represented by ε_p and f_p, roughly defines the difference between the elastic and inelastic buckling range. The cross-section will show post-buckling resistance if the elastic critical stress is less than the proportional limit ($\sigma_{cr} < f_p$). If local buckling or secondary buckling takes place, the cross-section will show post-buckling resistance until the critical stress for local buckling ($\sigma_{cr} < \sigma_{cr;l}$). The post-buckling resistance for distortional buckling is determined from:

Plate group I post-buckling resistance ($\sigma_{pm;pg1}$):

$$\sigma_{pm;pg1}(\varepsilon) = E\varepsilon \quad \text{for } \varepsilon < \varepsilon_{cr;d}$$

$$\sigma_{pm;pg1}(\varepsilon) = 0.66 E\varepsilon_{cr;d} + 0.36 E\varepsilon - 0.025 E \frac{\varepsilon^2}{\varepsilon_{cr;d}} \quad \text{for } \varepsilon_{cr;d} \leq \varepsilon \leq \min(\varepsilon_{cr;l}; \varepsilon_p)$$

$$\sigma_{pm;pg1}(\varepsilon) = 0.66 E\varepsilon_{cr;d} + 0.36 E\varepsilon_{cr;l} - 0.025 E \frac{\varepsilon_{cr;l}^2}{\varepsilon_{cr;d}} \quad \text{for } \varepsilon \in [\varepsilon_{cr;l}; \varepsilon_p]$$

Plate group II post-buckling resistance ($\sigma_{pm;pg1}$):

The plates of plate group II behave elastically up to either the proportional limit is reached, or secondary buckling occurs:

$$\sigma_{pm;pg2}(\varepsilon) = E\varepsilon \quad \text{for } \varepsilon < \min(\varepsilon_p; \varepsilon_{cr;2})$$

If secondary or local buckling occurs in the elastic range an additional post-buckling resistance is available:

$$\sigma_{pm;pg2}(\varepsilon) = 0.6 E\varepsilon_{cr;2} + 0.42 E\varepsilon - 0.015 E \frac{\varepsilon^2}{\varepsilon_{cr;2}} \quad \text{for } \varepsilon_{cr;2} \leq \varepsilon \leq \varepsilon_p$$

Predict the axial resistance ($N_{u;pm}$) as a function of ε

$$N_{u;pm}(\varepsilon) = \sigma_{pm;pg1}(\varepsilon)A_{pg1} + \sigma_{pm;pg2}(\varepsilon)A_{pg2}.$$

6   Comparison results

Table 3 presents the results of the FE-model, calculations based on Eurocode 9, Kutanova prediction model and the adapted Direct Strength Method for all considered C-shaped specimens applying material properties of the three aluminium alloys. The procedure for elastic buckling calculation with post-buckling strength is applied for eight specimens of alloy 6082-T6, for four specimens of alloy 6060-T66 and for one specimen of alloy 5083-H111. For all the specimens design approach for distortional buckling prediction is used except for the specimen 1(2)C10, where local-distortional interaction is considered.

Table 3: Calculation results for elastic distortional and local-distortional buckling prediction according to FEM, Eurocode 9, Kutanova model and the adapted Direct Strength Method for C-shaped profiles

Specimen	Material	FEM N[kN]	EC9 N[kN]	Kutanova model N[kN]	Adapted DSM N[kN]	AA N[kN]	EC9/FEM	Kutanova model/ FEM	Adapted DSM/FEM	AA/FEM
2.5(3)C5	6082-T6	100	81	101	91	73	0.81	1.01	0.91	0.73
1(2)C10	6082-T6	40	39	38	37	35	0.98	0.95	0.93	0.87
2(2.5)C5	6082-T6	69	57	73	64	49	0.83	1.06	0.93	0.71
1(2)C7.5	6082-T6	36	36	39	39	29	1.01	1.09	1.09	0.81
1.5(2)C5	6082-T6	44	38	43	40	30	0.87	0.98	0.91	0.70
1(2)C5	6082-T6	34	33	35	31	23	0.97	1.03	0.91	0.69
0.75(2)C5	6082-T6	30	30	29	25	21	0.99	0.96	0.83	0.70
0.75(1.5)C5	6082-T6	21	20	20	19	14	0.97	0.97	0.92	0.68
1.5(2)C5	6060-T66	34	29	34	33	24	0.85	0.99	0.96	0.71
1(2)C5	6060-T66	27	25	28	26	19	0.92	1.03	0.95	0.71
0.75(2)C5	6060-T66	24	23	22	21	18	0.96	0.92	0.88	0.74
0.75(1.5)C5	6060-T66	15	16	15	16	12	1.08	1.01	1.08	0.79
0.75(1.5)C5	5083-H111	12	13	13	13	10	1.05	1.05	1.05	0.81
						avg	0.94	1.00	0.95	0.74
						stdev	0.08	0.05	0.08	0.06

The FEM results are assumed to be the "true" values. According to the results of the comparison analysis, it can be summarized that the maximum deviation of the Kutanova prediction model is 9%, the maximum deviation of the adapted DSM is 17%, while the deviations of Eurocode 9 and AA specification can reach, respectively, 20% and 30%. Although the prediction model is the most accurate of the four methods it is sometimes a bit unconservative, which is however also the case for EC9 and DSM. Only AA is always safe but happens to be very conservative.

7 Conclusions

Cross-sectional instability often determines the structural resistance of aluminium members with slender cross-sectional shapes. Local and distortional buckling phenomena correspond to cross-sectional instability. The cross-sectional complexity makes the prediction of local and distortional buckling behaviour one of the most important design aspects. Current design rules for aluminium provide design rules for cross-sectional instability with limited accuracy. Therefore, an extensive study into local and distortional bucking has been carried in the recent past (Mennink [2002], Schafer [2006a], Kutanova [2009]). However, distortional buckling of aluminium structural members was not extensively investigated.

In the current paper, analytical approaches and current design rules for prediction the distortional buckling behaviour of C-shaped aluminium specimens are discussed. Distortional buckling is known as a flange-stiffener phenomenon. Therefore, distortional buckling is studied on C-shaped specimens. In case of distortional buckling, flange/lip assemblies or outstanding plate elements buckle first and belong to the supported group. The internal element provides initial support for outstanding elements. Local buckling of the internal plate is considered as secondary buckling of the cross-section. The secondary buckling of the internal plate can be predicted by the finite strip method. A perfect agreement is found between FSM and FEM results for secondary buckling of the supporting plate. Thus, the CUFSM results can be used for initial buckling prediction and also for secondary buckling prediction.

The Direct Strength Method cannot be used for aluminium because this method has been developed for distortional buckling of cold-formed steel. Thus, an adapted DSM method has been proposed.

The results of the finite element method are assumed to represent the reality. Comparing the results of analytical methods and the FE-model it can be concluded that the best prediction is provided by the Kutanova model (statistical results of Table 3). Calculation results based on the adapted Direct Strength Method gives a sufficient estimation, however rather conservative. The Eurocode 9 outcome can be very conservative, but provides in general rather good results due to the fact that C-type cross-sections are considered. AA specification results are very conservative. For more complex cross-sectional shapes, the current design rules underestimate initial buckling as calculations are based on the critical stresses of individual plates.

Literature

Kutanova, N., *Cross-sectional instability of aluminium extrusions with complex cross-sectional shapes*, Ph.D. thesis, Eindhoven University of Technology, 2009.

Schafer, B.W. Direct Strength Method Design Guide, *American Iron and Steel Institute*, Washington, D.C., USA, 2006a.

CEN, EN 1999-1-1, *Eurocode 9: Design of aluminium structures*, Part 1-1: General structural rules, Brussels, 2007.

The Specification for Aluminum Structures, *The Aluminum Association*, Washington, DC 2005.

Hancock, G.J. (1978). Local, distortional, and lateral buckling of I-beams. *J. Struct. Div.-ASCE* 104, 11: 1787–1798.

Schafer, B.W. CUFSM 3.11 Elastic buckling prediction, *Johns Hopkins University*, USA, 2006b.

Hendriks, A.N., Wolters, J.B.M. DIANA Finite Element Analysis, *TNO DIANA BV*, Delft, the Netherlands, 9.2 edition, 2007.

Mennink, J. Preliminary FEM-simulations on aluminium stub columns. TU/e internal report (BCO-Report 99.09), Eindhoven University of Technology, 1999.

Mazzolani, F.M. *Aluminium alloy structures, 2nd edition*, Chapman & Hall, London, UK, 1985.

Hancock, G.J., Kwon, Y.B. and Bernard, E.S. (1994) Strength design curves for thin-walled sections undergoing distortional buckling. *J. Constr. Steel Res.* 31(2-3): 169–186.

Schafer, B.W., Peköz, T., Direct strength prediction of cold-formed steel members using numerical elastic buckling solutions, *14th Int. Specialty Conf. on Cold-Formed Steel Structures*, St. Louis, 1998.

Standards of Australia and Standards of New Zealand, *Australian/New Zealand Standard on Cold-Formed Steel Structures*, AS/NZS 4600 (second edition), 2005.

Mennink, J., *Cross-sectional stability of aluminium extrusion*, Ph.D. thesis, Eindhoven University of Technology, 2002.

Kwon, Y.B., Hancock, G.J. (1992) Tests of cold-formed channels with local and distortional buckling. Journal of Structural Engineering (ASCE) 118(7): 1786–1803.